AGU PUBLICATIONS

JGR

Journal of Geophysical Research: Space Physics

REVIEW PAPER
10.1002/2016JA022579

Special Section:
Measurement Techniques in Solar and Space Physics: Particles

The "Puck" energetic charged particle detector: Design, heritage, and advancements

G. Clark[1], I. Cohen[1], J. H. Westlake[1], G. B. Andrews[1], P. Brandt[1], R. E. Gold[1], M. A. Gkioulidou[1], R. Hacala[1], D. Haggerty[1], M. E. Hill[1], G. C. Ho[1], S. E. Jaskulek[1], P. Kollmann[1], B. H. Mauk[1], R. L. McNutt Jr.[1], D. G. Mitchell[1], K. S. Nelson[1], C. Paranicas[1], N. Paschalidis[2], and C. E. Schlemm[1]

[1]The Johns Hopkins University Applied Physics Laboratory, Laurel, Maryland, USA, [2]NASA Goddard Space Flight Center, Greenbelt, Maryland, USA

Key Points:
- Review of the compact Energetic Particle Detector known as the Puck
- Puck EPD heritage includes five successful scientific missions
- Unexpected results and potential advancements of the Puck are discussed

Correspondence to:
G. Clark,
george.clark@jhuapl.edu

Citation:
Clark, G., et al. (2016), The "Puck" energetic charged particle detector: Design, heritage, and advancements, *J. Geophys. Res. Space Physics*, *121*, 7900–7913, doi:10.1002/2016JA022579.

Received 21 FEB 2016
Accepted 27 JUL 2016
Accepted article online 30 JUL 2016
Published online 30 AUG 2016

Abstract Energetic charged particle detectors characterize a portion of the plasma distribution function that plays critical roles in some physical processes, from carrying the currents in planetary ring currents to weathering the surfaces of planetary objects. For several low-resource missions in the past, the need was recognized for a low-resource but highly capable, mass-species-discriminating energetic particle sensor that could also obtain angular distributions without motors or mechanical articulation. This need led to the development of a compact Energetic Particle Detector (EPD), known as the "Puck" EPD (short for hockey puck), that is capable of determining the flux, angular distribution, and composition of incident ions between an energy range of ~10 keV to several MeV. This sensor makes simultaneous angular measurements of electron fluxes from the tens of keV to about 1 MeV. The same measurements can be extended down to approximately 1 keV/nucleon, with some composition ambiguity. These sensors have a proven flight heritage record that includes missions such as MErcury Surface, Space ENvironment, GEochemistry, and Ranging and New Horizons, with multiple sensors on each of Juno, Van Allen Probes, and Magnetospheric Multiscale. In this review paper we discuss the Puck EPD design, its heritage, unexpected results from these past missions and future advancements. We also discuss high-voltage anomalies that are thought to be associated with the use of curved foils, which is a new foil manufacturing processes utilized on recent Puck EPD designs. Finally, we discuss the important role Puck EPDs can potentially play in upcoming missions.

1. Introduction

The last Measurement Techniques in Space Plasmas conference occurred over 20 years ago and since then major discoveries of the plasma and energetic charged particle environments in our solar system and beyond have necessitated new instrument designs to push the scientific state of the art. Several terrestrial (e.g., Van Allen Probes) and planetary (e.g., Galileo and Cassini) missions have revealed the intricate links between the charged particle environment and the planetary environment as a whole. Similarly, the Voyager and Ulysses missions enhanced our understanding of the particle environment throughout the inner and outer heliosphere.

Charged particles with energies greater than tens of keV have at least two main functions. They can (1) be the more critical portion of the plasma distribution function in some processes and (2) act as tracers of magnetospheric and heliospheric processes in others. As tracers they can be used, for example, to infer circumplanetary neutral cloud densities at Jupiter and Saturn [e.g., *Lagg et al.,* 2003; *Paranicas et al.,* 2008, and references therein], to instantaneously determine whether the spacecraft is on open or closed magnetic field lines [e.g., *Williams and Frank*, 1980; *Scholer et al.,* 1981, 1982; *Mitchell et al.,* 2009], to remotely sense magnetic field boundaries [e.g., *Williams*, 1979; *Oksavik et al.,* 2002], and to sense bulk speeds of the flowing cold plasma using the Compton-Getting effect [e.g., *Kane et al.,* 1998; *Paranicas et al.,* 2005] or via the dispersion of magnetospheric injections [e.g., *Mauk et al.,* 2005; *Clark et al.,* 2016]. Energetic particles are also a primary result of magnetic reconnection [e.g., *Hoyle*, 1949; *Zelenyi et al.,* 1990], are key indicators of magnetospheric loss processes [e.g., *Sibeck et al.,* 1987; *Sibeck and McEntire*, 1988; *Krupp et al.,* 2002], and drive auroral emissions [e.g., *Mauk and Bagenal*, 2012]. On the other hand, particles above 10 keV can dominate moments of the particle distribution function (e.g., the particle pressure) in large parts of Jupiter's magnetosphere [e.g., *Bagenal and Delamere*, 2011; *Mauk et al.,* 1996] and contribute important forces that sustain Jupiter's magnetodisk configuration [*McNutt*, 1983; *Mauk and Krimigis*, 1987; *Paranicas et al.,* 1991; *Nichols et al.*, 2016]. Some physical phenomena would not exist without these particles, such as auroral X-ray emissions [*Cravens et al.,* 1995] and some outer planetary auroral emissions at other

wavelengths [e.g., *Saur et al.,* 2006]. Energetic charged particles are a driver of deep surface modifications on icy satellites such as in *Howett et al.* [2011] and *Paranicas et al.* [2014]. Interstellar pickup ions are produced from interstellar gas, and local measurements can be used to constrain the global gas distribution [*Gloeckler and Geiss,* 2004].

This list of the ways in which energetic charged particles play a central role in auroral, magnetospheric, and other processes, or as tracers of both local and global magnetospheric processes, is by no means exhaustive, and we refer the reader to the following review papers on charged particle dynamics [*Johnson*, 1990; *Jokipii,* 2001; *Kunow et al.,* 1991; *Richardson*, 2004]. It is clear that diagnosing the charged particle environments is in many cases the only method of understanding some physical phenomena. Improving measurements (e.g., determining pitch angle distributions at sufficient resolution to satisfy the science goals) requires the use of emerging technologies and electro-optical designs to push the state of the art.

It is our view that the measurement of flux with angular knowledge by species, at sufficiently high energy, pitch angle, and time resolution, is the most ideal situation. In this paper, we will focus on charged particles above 1 keV in energy. These are particles whose net motion is not bound (with increasing energy) by the electric field. From a measurement perspective, a distinction exists between these particles and the cold or warm plasma ($<$1 keV) because historically it has been difficult to construct a single sensor with a dynamic energy range to measure the full energy distribution of space plasmas. In this review we intentionally omit discussing low-energy plasma instrumentation; however, we suggest the following review articles and references therein: *Hughes and Rojansky* [1929], *Johnstone* [1972], *Young et al.* [1987], *Young et al.* [1988], *Wolfe et al.* [1966], *Paschmann et al.* [1985], *Duvet et al.* [2000], *Kasahara et al.* [2006], *Allegrini et al.* [2009], and *McComas et al.* [2013].

Space-based energetic charged particle sensors date back to the late 1950s, when *Van Allen* [1958] used a Geiger-Müller counter on board Explorer 1 to measure ions ($>$ ~30 MeV) and electrons ($>$ ~3 MeV) in Earth's orbit. This effort led to the discovery of Earth's radiation belts, or the Van Allen radiation belts, which solidified the importance of measuring space plasmas. Since the late 1950s, energetic particle sensors evolved into more complex systems and required novel designs to handle the space environment (i.e., increase the signal-to-noise ratio and expand the dynamic range). Eventually, these instruments were able to measure the time variation, energy distribution (over a large range), angular distribution, and the composition of the charged particle environment, which transformed our understanding of the physical links between charged particles in a planetary or heliospheric system. Here is a list of some of the previous energetic particle instruments that made significant scientific contributions to our understanding of Earth's, Saturn's, Jupiter's, Uranus', Neptune's, and our Heliospheric environment: Low-Energy Charged Particle Experiment [*Krimigis et al.,* 1977], the Cosmic Ray System [*Stone et al.,* 1977], the Medium-Energy Particle Analyzer [*McEntire et al.,* 1985], Energetic Particle Detector [*Williams et al*., 1992], the Galileo Heavy Ion Counter [*Garrard et al.,* 1992], Energetic Particle and Ion Composition [*Williams et al.,* 1994], Electron, Proton, and Alpha Monitor [*Gold et al.,* 1998], the Magnetosphere Imaging Instrument [*Krimigis et al.,* 2004], and the Time History of Events and Macroscale Interactions during Substorms Solid-State Telescopes [*Sibeck and Angelopoulos*, 2008].

In the 1990s there was a trend to make instruments better, cheaper, and faster [*Young*, 1998]. This trend resulted in the development of instruments that were smaller and less power hungry yet could meet complex science objectives. Responding to this movement and conservative design requirements imposed by missions such as NASA's New Horizons and MErcury Surface, Space ENvironment, GEochemistry, and Ranging (MESSENGER), the Johns Hopkins University Applied Physics Laboratory (APL) developed a new type of compact Energetic Particle Detector (EPD), which is colloquially known as the "hockey puck" or puck because it resembles an ice hockey puck in size [*McNutt et al.,* 2008]. The Puck EPD was designed to measure energetic electrons, protons, and heavy ions (typically greater than tens of keV to a few MeV). It achieved this through a compact design that consisted of time of flight (TOF) section to measure the ion's velocity and an array of solid-state detectors (SSDs) to measure the total deposited energy of an incident electron or ion. Since the first development of the Puck EPD for NASA's MESSENGER mission to Mercury [*Andrews et al.,* 2007], the Puck EPD has flown on four subsequent NASA missions [*Mauk et al.,* 2013; *Mitchell et al.,* 2013; *Mauk et al.,* 2014] with great success. The design of the Puck EPD has evolved since it was initially conceived a decade ago, and here in this review article we summarize its design, unexpected results, new advancements, and the prospects of Puck EPD instruments for future missions.

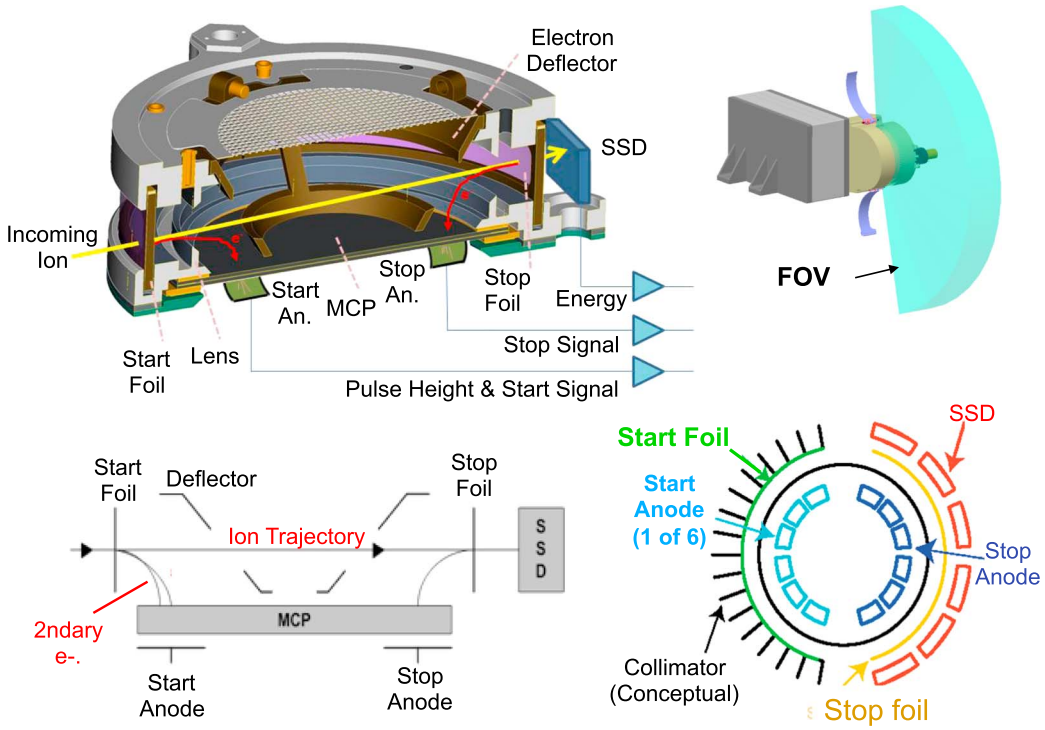

Figure 1. Schematic illustrations of the Puck EPD and its various components.

2. Design

Here we describe the general design and operation of the Puck EPD. We note that there are some small differences, however, between the earlier versions of the Puck and the latest generation. In an effort to be succinct, we focus on the design of the latest generation for this section and highlight some of the differences in the heritage section.

These sensors are designed to perform the following measurement functions: (1) to measure the angular and energy distributions of energetic electrons; (2) to identify incident ions (i.e., determine mass and energy) and characterize their angular distribution; (3) have a large dynamic range that can span four to five decades in intensity for particles in the energy range between ~10 keV and > 1 MeV; and (4) to suppress background (i.e., detector counts that are outside the nominal energy and pitch angle range of the target species) caused by UV and penetrating radiation. Figure 1 illustrates how these basic measurement functions are performed. Generally speaking, particles (electrons and ions) enter the aperture of the sensor, pass through a series of foils in the TOF chamber, and then implant their energy into the SSD. These three components provide the angular information, ion identification, and incident energy while simultaneous reducing solar light, UV, and other backgrounds such as the high-density low-energy plasma. Next, we describe the various components in more detail.

2.1. Aperture

The Puck EPD has a fan-like aggregate acceptance angle that spans 160° × 12°, which is collimated by a series of nested plates, each with an array of aligned holes. This design was necessitated because the instrument field of view is used to measure both electrons and ions. Thus, the collimator traps scattered electrons, minimizing the error in the pitch angle determination. Figure 2 depicts the collimator design and response function that was utilized by the Jupiter Energetic Particle Detector Instruments (JEDI) sensor [*Mauk et al.*, 2013]. JEDI consists of a series of five concentric blades of a Tungsten-Copper (WCu) mixture. The middle blade holds the collimator foil —a 350 Å aluminum foil—which was implemented to suppress both "out-of-passband" low-energy electrons and solar light and UV. The latest generation of Pucks consists of similar apertures; however, their hole patter and shape may differ. As noted in *Mauk et al.* [2013], the design is balanced by considering the geometry

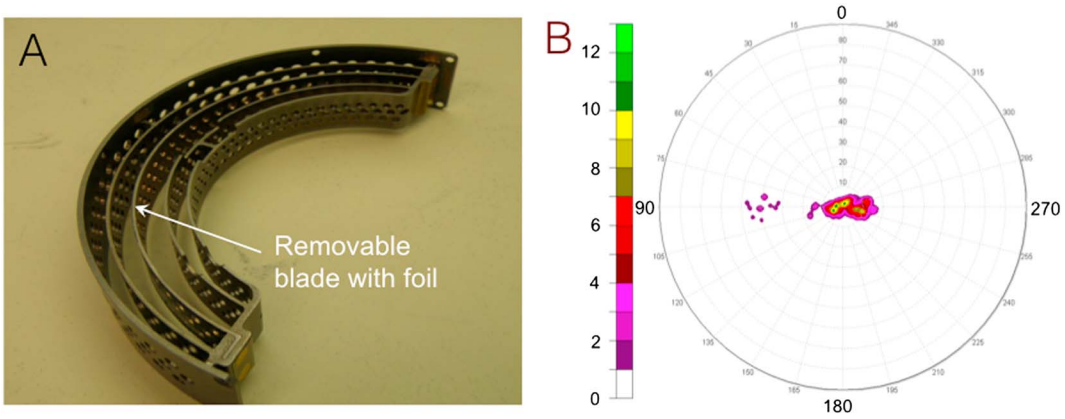

Figure 2. The Juno-JEDI (a) multihole collimator and the (b) viewing response of the collimator. The main response is depicted by the central peak, and the scattering of points to the left represents the side lobes (~1% of the main response).

needed for a particular mission and minimizing the side lobes of the aperture. The side lobes are depicted in Figure 2b for the JEDI collimator. The primary response function of the collimator is contained in the central blob, whereas the sprinkling of points to the left represents the side lobe (1% of the main response).

2.2. Time of Flight Chamber

The purpose of the TOF chamber (Figure 1) is used primarily to determine ion speed between the start and stop foils. This measurement is used with other parameters to identify the particles mass and thus composition. Because of this reason, no TOF analysis is needed for electrons. The TOF chamber in the Puck is a cylindrically symmetric chamber composed of a start foil, a stop foil, an electrostatic lens, and a microchannel plate (MCP) with segmented current collectors. As the primary ion passes through the collimator, it first interacts with the start foil and then the stop foil. Secondary electrons are generated as a result of the ion passing through the foils and then are subsequently steered to the MCP by the electrostatic lens. The MCP lies above an anode which is segmented into a start and stop region corresponding to the stop and stop foils. Moreover, each segmented anode has individual pads corresponding to each look direction. The stop and stop sections are essential to differentiate between the start and stop signals generated by the secondary electrons on the start and stop foils. In other words, the timing difference between these signals provides the time it takes for the ion to pass through the TOF chamber. The discrete anode pads facilitate in correcting for accidental rates and errors in the TOF. To note, some of the Puck EPDs have an additional foil within the collimator that is biased such there is a moderate (kV range) negative potential between the collimator foil and start foil. This setup results in a skewed TOF distribution for low-energy ions because the ion's charge state is redistributed as it passes through a foil. For example, a 10 keV proton has only a 20% probability of remaining charged as it exits the foil. This means that the neutralized component is unaffected by potential drop, and thus, the TOF distribution can be board compared to the low-energy incident ion. A compilation of curves describing charge state distributions through foils can be found in *Allegrini et al.* [2016].

The Puck EPD generally employs two methods to determine ion composition: the TOF by Energy (TOF × E) method and/or the TOF by MCP-Pulse Height (TOF × PH) method. The TOF × E method requires that the ion's energy can be measured independently in the solid state detector and combined with the coincident TOF measurement to derive the particle mass from the kinetic energy expression. This is the preferred method to identify particle species with the Puck EPD; however, it does not work well below ~20 keV for protons due to the limitations of the discrimination in the energy system. For these lower energies the TOF × PH method is used. In this method the velocity is determined by the particle's TOF, and the mass is determined by the pulse height recorded from MCP detection system. The mass separation is somewhat coarse using the MCP pulse height method, and therefore, only reliably separates protons from heavy ions. This method has been used on the IMAGE high-energy neutral analyzer (HENA) instrument [*Mitchell et al.,* 2003] (Figure 3b); however, it has not been successfully demonstrated on the Puck EPDs. We discuss this point further in section 5. The TOF × E and TOF × PH methods are depicted in Figures 3a and 3b, respectively. It can be seen in Figure 3a that species separation between the heavy ions becomes more difficult at lower energies.

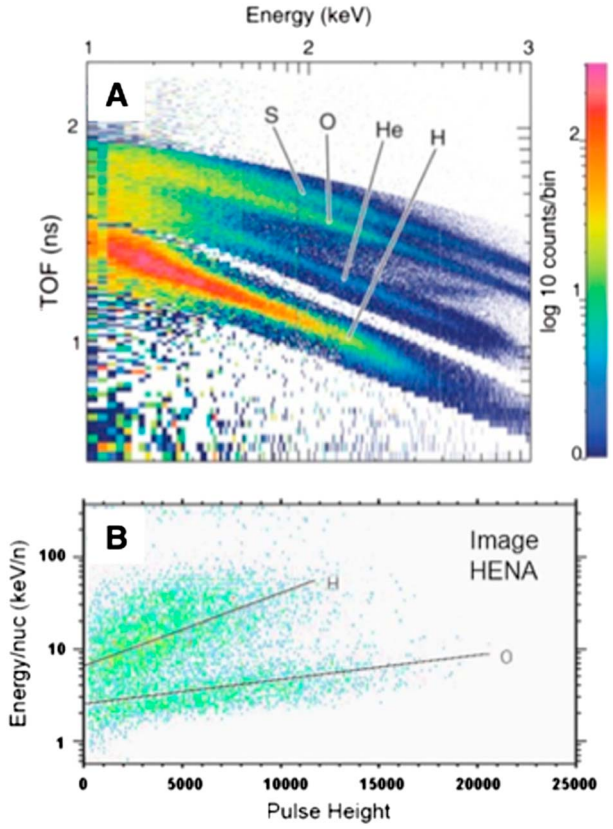

Figure 3. (a)TOF × E measurements made by the PEPSSI instrument during the Jupiter flyby in 2007. Clear separation of H, He, O, and S at energies above ~200 keV. Separation of H, He, and O + S at energies below ~200 keV. (b) Energy/nucleon (calculated by the TOF) × PH measurements made at Earth from the IMAGE-HENA instrument. MCP Pulse height analysis can be used to distinguish between H and O (Figure 3b).

2.3. Solid State Detectors

A single SSD from the JEDI sensor is shown in Figure 4 and is representative of the other latest generation Pucks (e.g., Radiation Belt Storm Probes Ion Composition Experiment (RBSPICE) and Energetic Ion Spectrometer (EIS)). Each SSD is approximately 500 μm thick and consists of electron and ion pixels, which are both segmented into small and large pixels. The electron pixels are covered with an aluminum flashing that is ~2 μm thick. Low-energy ions (< ~250 keV) cannot penetrate the flashing, thus allowing better discrimination of electrons from ions. Furthermore, the SSD output is discriminated around 20 keV, which means clean electrons measurements begin around 25 keV. The ion pixels do not have the aluminum flashing but are optimized with a thin dead layer of ~50 nm. The large pixels are roughly a factor of 20 larger than the small pixels, which corresponds to factor of 20 in sensitivity. Thus, the Puck EPDs can increase or decrease their sensitivity by effectively changing their collecting area and therefore drastically increasing their dynamic range. The SSD is attached to a hanger made of WCu and is ~0.25 cm thick. In addition to holding the SSD and the small application-specific integrated circuit (ASIC) board on the back, the hanger also provides some shielding to penetrating radiation.

2.4. Backgrounds

To improve the success of making high-fidelity measurements, one must be cognizant in the design phase of the backgrounds and environmental challenges present. The SSD and MCP detectors are sensitive and require to be properly shielded from solar light and UV, penetrating radiation, cosmic rays, and "out-of-band" plasma. The latest generation of Puck EPDs (heritage is further discussed in the next section) includes the aforementioned collimator foil, which in this context facilitates in blocking solar light and UV as well as scattering the out-of-band plasma ions and electrons into the collimator. Another layer of defense against solar light and UV is the filtering with the thin start and stop foils used for secondary electron production. Since UV can generate spurious counts on the MCP and visible light can raise the noise level on the SSD, then it is important to select a foil thickness that can appropriately shield unwanted light. The start foil is a 50 Å carbon/350 Å polyimide/50 Å carbon foil and the stop foil is composed of 50 Å carbon/350 Å polyimide/50 Å carbon/ 200 Å aluminum. Lastly, to reduce the effects of penetrating radiation (high-energy ions and electrons and cosmic rays) shielding is placed around the SSDs (amount varies with instrument). Additionally, two of the Puck EPDs, namely, RBSPICE and JEDI, include "witness" detectors—an electron SSD pixel with a thick shield—that effectively turns it into a radiation monitor because it is only sensitive to > 1 MeV electrons and > 10 MeV ions.

Background rates can also be suppressed by requiring careful selection of the coincidence timing windows on the TOF start, TOF stop, and SSD pulses. The valid event rate can be calculated by [*Mitchell et al.,* 2013]

$$R_{VE} = R_{start} \times R_{stop} \times R_{SSD} \times t_{TOF} \times t_{SSD} \quad (1)$$

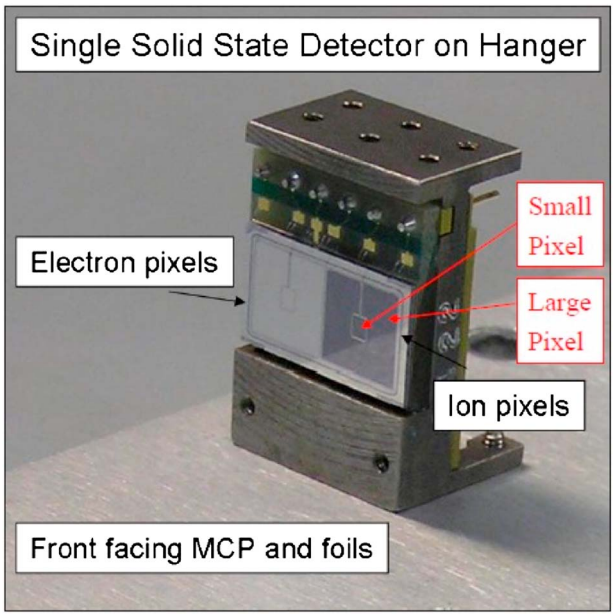

Figure 4. A single SSD from the Juno-JEDI instrument. Each SSD has four pixels: a large and small electron pixel and a large and small ion pixel. The hanger is approximately 0.25 cm thick, and attached on the back of the SSD hanger is the ASIC board.

where R_{start}, R_{stop}, and R_{SSD} are the rates on the start foil, stop foil, and SSD, respectively. Furthermore, t_{TOF} is the timing window between the start and stop TOF, and t_{SSD} is the timing window on the SSD pulse. Timing windows for the TOF circuitry are typically between 100 and 200 ns, and the timing pulse on the SSD is usually less than 1 μs. Assuming a modest background rate (i.e., $R_{start} \times R_{stop} \times R_{SSD}$) of 10^4 counts per second (c/s), $t_{TOF} = 100$ ns and $t_{SSD} = 1$ μs then equation (1) yields a valid event rate of ~0.1 c/s. Therefore, even for a very low foreground rate of just 1 c/s, the predicted background rate is still decade below the foreground. Here we chose arbitrary values based on experience with Earth's environment to illustrate the effectiveness of properly selecting the coincidence timing windows based on design requirements of the instrument.

3. Heritage

Figure 5 shows the various Puck EPDs designed and built at Johns Hopkins University/APL. The first Puck EPD was the Energetic Particle Spectrometer (EPS), part of the Energetic Particle and Plasma Spectrometer package on the MErcury Surface, Space ENvironment, GEochemistry, and Ranging (MESSENGER) mission [*Andrews et al.,* 2007]. In addition to implementing the single-MCP TOF chamber and six telescopes, this initial instrument also introduced the capability to switch between large and small SSD pixels to enable high-sensitivity or high-rate observations, respectively. Unfortunately, the EPS instrument suffered from a malfunction in the TOF system attributed to a design flaw in the MCP holder, which prevented adequate biasing of the MCPs. The instrument's energy measurements were unaffected, however, and the sensor returned valuable ion/electron energy measurements at Mercury. It was able to determine unambiguously that Mercury's small magnetosphere is dominated by low-energy electrons instead of the high-energy ions as reported by Mariner 10 [*Ho et al.,* 2011, 2012].

The next iteration of the Puck EPD was the Pluto Energetic Particle Spectrometer Science Investigation (PEPSSI) instrument on the New Horizons spacecraft [*McNutt et al.,* 2008]. PEPSSI presented different requirements than EPS with respect to available power and maximum count rates. While larger rates were anticipated for the Jupiter flyby calibration opportunity, the requirements were always focused at the conditions at Pluto. The combination of lower expected counting rates and the need to save power led to the implementation of (1) lower current MCPs, (2) improved efficiency in both the low-voltage power supply and high-voltage power supply, (3) a complete redesign of the energy board using new application-specific integrated circuit (ASIC) chips [*Paschalidis*, 2006], and (4) a redesign of the time of flight (TOF) board with different amplifiers and delay lines to achieve higher gain [*Paschalidis et al.,* 2002]. With the need for long-term reliability during the cruise to Pluto, PEPSSI added a high-voltage (HV) safing system to shut down the supply if the HV current exceeds a threshold. The EPS instrument used 24 detector pixels (six large for ions, six large for electrons, and the same counts with small ones), whereas PEPSSI uses only 12 pixels (nine large ions and three large electrons). One of PEPSSI's sectors also includes an alpha source of degraded ^{241}Am. This source turned out to be useful for in-flight calibration and tracking the change of efficiency over time.

Following PEPSSI, a new generation of Puck EPD instruments was developed nearly simultaneously. This cohort was composed of the Jupiter Energetic Particle Detector Instruments (JEDI) for the Juno mission to Jupiter [*Mauk et al.,* 2013], the Radiation Belt Storm Probes Ion Composition Experiment (RBSPICE) on the

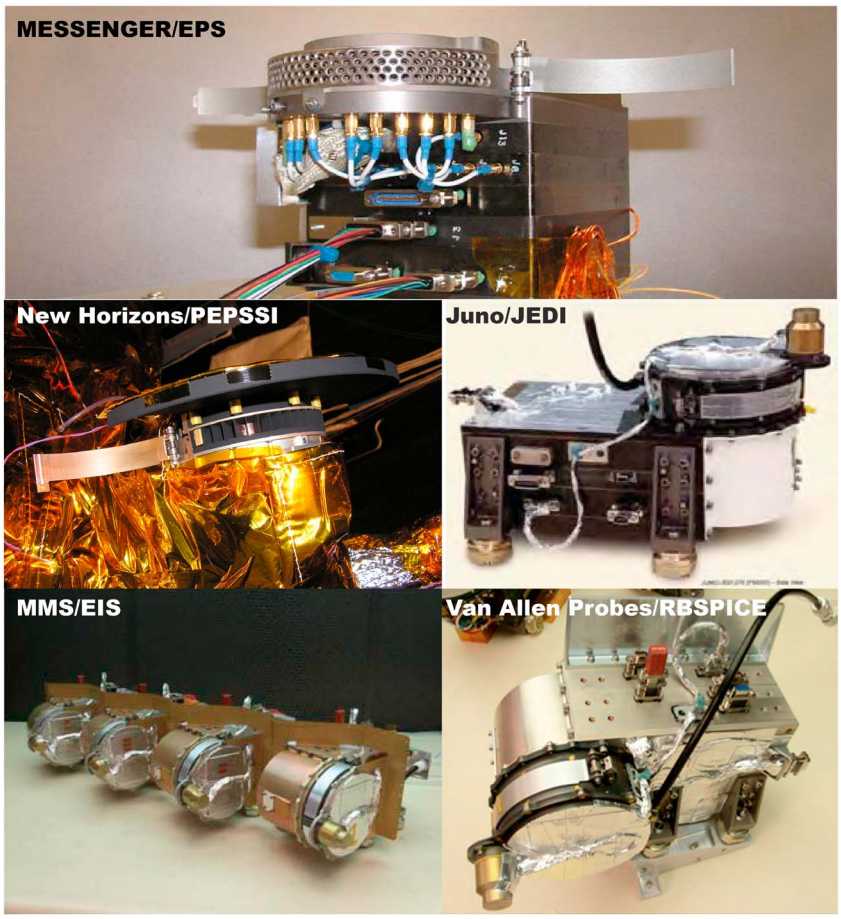

Figure 5. The various Puck Energetic Particle Detectors.

two Van Allen Probes spacecraft [*Mitchell et al.,* 2013], and the Energetic Ion Spectrometer (EIS) on the Magnetospheric Multiscale (MMS) mission [*Mauk et al.,* 2014]. This new version maintained the traditional Puck EPD optics while implementing substantial changes to the mechanical and electrical designs. Major advancements include the separation of the optics and electronics into wholly separate subsystems, and the relocation of the ASIC energy preamps to the back of the SSDs, and timing preamps to the back of the anode board; colocating the preamps with the sensor yielded a significant improvement in noise performance. Because the high electron intensities within the magnetized magnetospheres of Jupiter and Earth posed the threat of disrupting the measurement of the ions by overwhelming the start pulse processing circuitry, these later Pucks introduced a collimator comprised of five cylindrically shaped blades with multiple aligned holes and added a third 350 Å aluminum "collimator" foil upstream of the "start" foil to scatter low-energy particles. Additional modifications included an improved custom power supply as well as the use of the field-programmable gate array-embedded APL-developed Scalable Configurable Instrument Processor and coating the start and "stop" foils with carbon instead of aluminum to improve secondary electron yield. This group of Puck EPDs also benefitted from an increased separation between the stop foil and SSDs yielding much improved noise performance.

While the nonspinning MESSENGER and New Horizons spacecraft limited the pitch angle coverage of EPS and PEPSSI, these later Puck EPDs were able to take advantage of their spinning spacecraft to ensure measurement of full pitch angle distributions. For example, to allow for nearly simultaneous observation of the full pitch angle distribution, two JEDI instruments were mounted with their multiple apertures in the plane perpendicular to the Juno spacecraft's spin axis. A third instrument aligned parallel to the spin axis allows for measurement of the full three-dimensional distribution every spin. Conversely, single RBSPICE and EIS instruments are mounted on each spacecraft, parallel to the spin axis, and thus obtain a full pitch angle distribution once per spin.

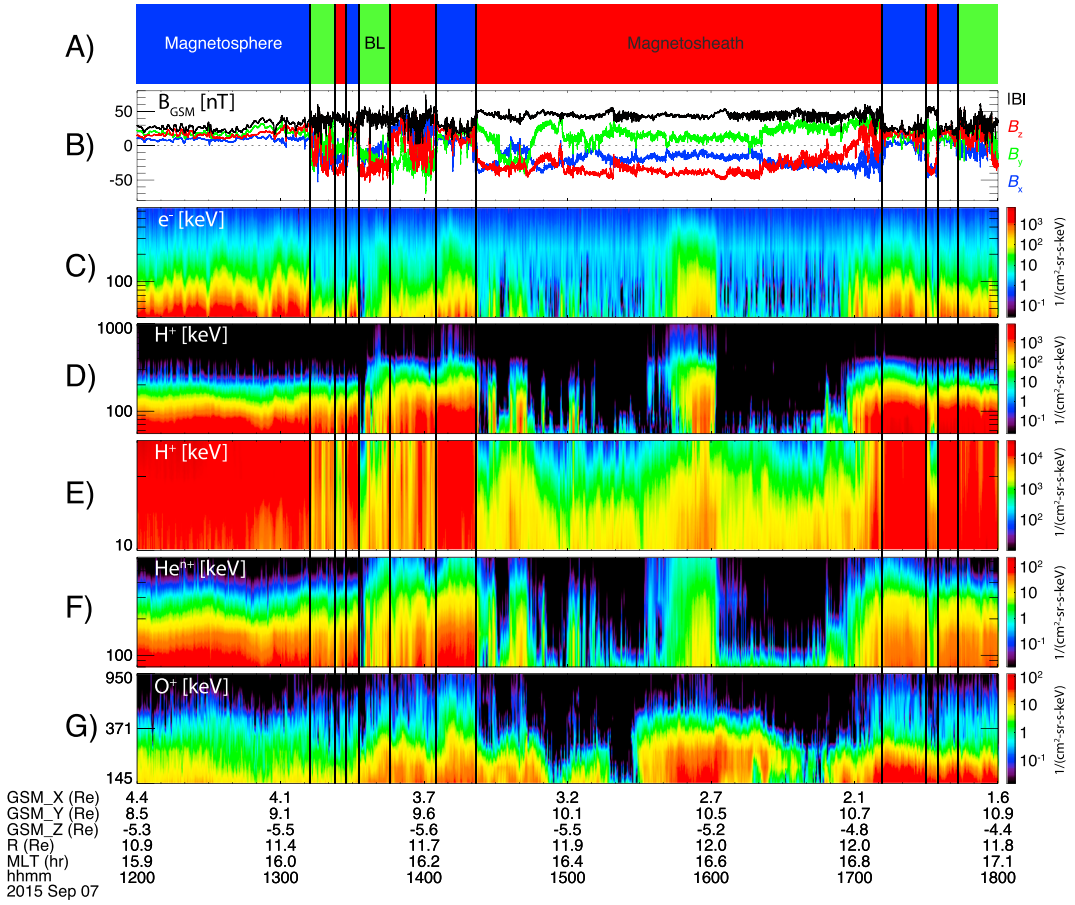

Figure 6. Measurements from the EIS instrument onboard MMS [*Cohen et al.,* 2016]. Figures 6c and 6d illustrate the various measurement techniques and in-flight performance of the Puck EPD.

4. In-Flight Performance

The Puck has and continues to play a valuable role in diagnosing space plasmas both in planetary and heliospheric environments. In this section we highlight a few examples from the most recent missions and provide a table in Appendix A containing most of the publications using data from the Puck.

Figure 6 illustrates the various measurement capabilities of the Puck with data from the MMS-EIS [*Cohen et al.,* 2016]. Figure 6c shows the electron measurements from the large pixel electron SSD. The faint feature of approximately a few counts per second around 200 keV is believed to arise from penetrating radiation. Cosmic rays can easily pass through the SSDs leaving behind a constant and calculable amount of deposited energy, which happens to be ~200 keV due to the dimensions of the SSDs used in EIS. This is one clear illustration on how backgrounds manifest into the measurement but can also be removed in a trivial manner if properly understood.

Figures 6d–6g illustrate the following measurements, respectively: protons by the TOF × E method (d); protons by the TOF × PH method (e); helium ions by the TOF × E method (f), and oxygen ions form the TOF × E method. The cosmic ray track is not seen in these data because the TOF × E and TOF × PH methods use coincidence logic between the TOF pulses and the SSD pulses. Figures 6d and 6e illustrate the overlap and agreement between the TOF × E and TOF × PH method, which allows clean proton measurements from slightly less than ~10 keV to greater than ~1 MeV.

Other examples include RBSPICE observations that have shown multiple mesoscale injections observed deep into the inner magnetosphere in storm main phase provide a major (>30%) contribution to hot plasma pressure [*Gkioulidou et al.,* 2014]. Furthermore, *Ukhorskiy et al.* [2014] used RBSPICE measurements to show that

energetic electrons (<1 MeV) across the entire inner radiation belt (<3 R_E) are organized in regular patterns, named "zebra stripes," which are thought to be the result of diurnal oscillations of the inductive electric field induced by Earth's rotation. Meanwhile, early measurements from EIS demonstrate an unprecedented level of energetic particle dynamics at the dayside terrestrial magnetopause [e.g., *Anderson et al*., 2016; *Cohen et al.,* 2016]. Finally, the Juno-JEDI instrument is expected to unveil new clues about auroral acceleration and magnetosphere-ionosphere coupling at Jupiter. Juno will begin its orbit insertion on 4 July 2016. In the meantime, during its cruise phase in interplanetary space, the JEDI instruments have observed energetic particle events far upstream (nearly 1 AU) of Jupiter's magnetosphere. Analysis is still ongoing at this time; however, since such few observations exist upstream of Jupiter's bow shock, we expect to learn something new about the process governing ion escape and acceleration in planetary magnetospheres.

5. Unexpected Results from Prior Implementations

5.1. Microdischarges

The new generation of Puck EPDs has experienced challenges with microdischarges believed to result from foil anomalies. It should be noted that the Puck EPD is the first instrument to utilize curved foils. Curved foils may introduce certain unique complexities including structural vulnerabilities associated with nonuniformities and the creation of air pockets along the perimeter of the support structure during foil adhesion. Either of these factors could lead to the presence of small amounts of foil chad within the sensor volume or nonopaque regions in the foils that allow large amounts of plasma through, both of which could contribute to microdischarges. These foil anomalies are further exacerbated by the application of high voltage on the collimator foil. Future Puck EPDs are considering the use of flat, segmented foils in an effort to mitigate these complexities. An alternate hypothesis is that the cylindrical symmetry of the sensor volume leads to acoustic resonance during vibrational stresses that could compromise the foils. The significant differences in design of other instruments currently under development [i.e., *Mitchell et al*., 2016; *Hill et al*., under revision, 2016] address these vulnerabilities, as will future implementations of the Puck EPD. It should be emphasized that despite these anomalies and the resulting need for some operational nursing, all of the Puck EPD experiments are on track for achieving full scientific success.

5.2. High Voltage on Start and Stop Foils

As a matter of convenience (that is, running the MCP anode at ground potential), as well as an attempt to keep thermal plasma electron fluxes out of the sensor, we chose to run the Start (and Stop) foils at high negative potential (~−2.5 kV). In retrospect, we do not regard this as a good choice, because this made the sensor sensitive to environments with high plasma densities (especially in the ionosphere), as ambient cold protons are accelerated with enough energy to penetrate the Start foil and drive high rates on both Start and Stop. Additionally, this design puts a high-voltage element (the Stop foil) quite close to the sensitive SSD input surfaces, where noise from the foil HV supply can couple easily into the SSD front end amplifiers. Although this latter potential problem was overcome through sufficient filtering of the HV, holding the Stop foil at Ground would have been simpler. For future versions of this sensor we would revert to the procedure in our previous instruments of holding the Start and Stop foils near or at Ground.

5.3. TOF × PH Performance

In the pucks, as expected, oxygen does produce a statistically higher MCP pulse height than hydrogen, however because the spread in pulse heights is large for both species, the high pulse height tail of the hydrogen distribution significantly overlaps the mean of the oxygen distribution, while the low pulse height tail of the oxygen distribution lies on top of the mean pulse height of the hydrogen distribution. This results in poor separation of the species, with the potential for counts from either species contributing significantly to counts assigned to the other. For example, if a pulse height threshold is set as a discriminator between oxygen and hydrogen, in an environment entirely dominated by hydrogen the high pulse height tail of the hydrogen distribution will be interpreted by the onboard software as oxygen. Likewise, in an environment dominated by oxygen, the low pulse height tail of the oxygen will be interpreted as hydrogen. Because the distributions on HENA and INCA were sufficiently well separated from one another, the overlap in the distributions only contributed minor distortions in the composition. On the pucks, likely because the primary particle does not impact the MCP directly, the distributions of hydrogen and oxygen overlap to the extent that no clear minimum can be observed in the resultant pulse height distribution.

Table 1. The Five Puck EPDs and Their Characteristics

Mission	Instrument	Mass	Power	Energy Range (Ion)	Energy Range (Electron)	Composition	Energy Resolution	Time Resolution	Angular Resolution	Geometric Factor
MESSENGER	EPS [*Andrews et al.,* 2007]	1.5 kg	3 W	25–3000 keV (H), 35–3000 (He), 70–3000 keV (CNO),120–3000 keV (Fe)	25–1000 keV	H, He, CNO, Fe, e^-	~30–35%	0.5 s	22.5° × 12°	~0.03 cm^2−sr
New Horizons	PEPSSI [*McNutt et al.,* 2008]	1.5 kg	2.5 W	~1 keV/n to 1 MeV/n	25 to 500 keV	H, He, CNO, Fe, e^-	~25%	0.5 s	25° × 12°	0.15 cm^2−sr
Juno	JEDI [*Mauk et al.,* 2013]	6.4 kg	2 W	10–2000 keV (H), 25–2000 (He), 45–10000 keV (O/S)	25 to 1000 keV	H, He, O, S, e^-	20%	0.5 s	18° using rotation	0.004 cm^2−sr
Van Allen Probes	RBSPICE [*Mitchell et al.,* 2013]	6.6 kg	2 W	10–2000 keV (H), 25–10000 (He), 40–10000 keV (O/S)	25 to 1000 keV	H, He, O, e^-	20%	0.33 s	15° × 12°	0.0036 cm^2−sr
MMS	EIS [*Mauk et al.,* 2014]	2.2 kg	2 W	~20–> 500 keV (H), ~130–> 500 keV (O)	25 to 1000 keV	H, He, O, e^-	20%	~2.5 s (survey mode), ~0.625 s (burst mode)	26.7° × 12°	0.012 cm^2−sr

6. Potential Advancements

Here we discuss the benefits of advancing other aspects of the Puck EPD design, making use of emerging technologies and novel electrooptical designs. Additionally, many of these improvements allow for broader scientific investigations while addressing increased pressure to minimize instrument demand on spacecraft resources.

6.1. Improving Scattering and Energy Loss

For several decades now carbon foils have become a core technology in TOF systems due to their secondary emission characteristics and good angular and energy loss qualities [*McComas et al.,* 2004]. Improving these attributes requires making the foils thinner; however, there is a practical limit that is reached with current technologies due to structural integrity [*Allegrini et al.,* 2015, and references therein]. This current limit is somewhere around 0.5 $\mu g/cm^2$ or 100 atoms thick for thin carbon foils. Recent measurements in material science have revealed that graphene, a 2-D sheet of covalently bonded carbon atoms, is the strongest material ever measured [*Lee et al.*, 2008]. Therefore, graphene can be used to produce finer foils and thus improving the scattering and energy loss. Graphene's application to space-based instruments is an area of active research [e.g., *Allegrini et al.,* 2015, 2014; *Ebert et al.,* 2014]. Results show promise and have the potential to improve the sensitivity of the Puck EDP (larger particle throughput) and extend its measurement capability to lower energies.

6.2. Extending the Energy Range of the Puck EPD

The Puck EPD has traditionally exhibited a lower energy cutoff around 10 keV (cf. Table 1) due to the use of foils and SSDs. It is advantageous, however, to modify the design such that lower energy ions can be measured at the same time as the higher-energy ions. Bridging this energy range would potentially include the addition of an electrostatic analyzer to the Puck EPD design. One benefit would be the ability to measure solar wind protons (~1 keV), heavy ions (few keV and above), and pickup ions (few keV to several tens of keV) simultaneously. Other benefits may be the addition to measure corotational flows (order of 100 eV) in planetary magnetospheres and the ionic charge state of heavy ions [*Clark et al.,* 2016]. Currently, the Southwest Research Institute is attempting to cover this energy regime though an instrument design coined the Compact Dual Ion Composition Experiment [*Desai et al.,* 2015]. The novelty of this design utilizes a common TOF × E subsystem sandwiched between an electrostatic analyzer and an energetic particle sensor that measures ions between ~0.01 keV/q to ~10 MeV. Current instrument methods require the use of foils for the TOF measurement and detectors that are inherently energy dependent to measure the total ion energy. For example, low-energy ions are required to be significantly post accelerated such that they avoid being implanted into the foil and so they can deposit enough energy into the SSD to be registered. Progressive methods in ion detection and TOF tagging should be of high priority for future technology development.

6.3. Improving the Identification of Penetrating Particles

With the current design, there is an ambiguity between hundreds of keV electrons that deposit all their energy in the SSD and electrons of much higher energy that deposit a similar energy but penetrate through the SSD. Currently, the JEDI Puck make use of "witness detectors"—SSD pixels that are blocked by ~2 mm of Al to shield low-energy particles—to distinguish between low-energy particles from high-energy penetrators. However, future designs may consider adding a second layer of SSDs. Only the highest electron energies will trigger the second SSD. Such a second SSD layer will also remove accidentals in high rate environments and has the potential to further constrain the species identification.

7. Applications

Below we now outline a few scientific questions of high interest that can be addressed with the current Puck EPD and its potential advancements.

1. *Uranus*. Exhibits a unique magnetospheric configuration that raises interesting questions on particle transport, trapping, and satellite weathering. A Uranus Orbiter White Paper outlines the following: How stable are the Uranian radiation belts? What are the relative roles of moon sweeping and wave-particle interactions in limiting the radiation belt fluxes? What role do energetic charged particles play in creating the observed leading/trailing surface darkening asymmetries?
2. *Jupiter and Saturn*. Jupiter's magnetosphere will be explored by the three Juno/JEDI detectors. They can separate measured flux by species, energy, and pitch angle but do not discriminate among the fourth attribute, charge state. *Clark et al.* [2016] have shown the significance of this parameter in diverse subjects such as inferring neutral densities and understanding dynamic processes.
3. *Inner and outer heliosphere*. The heliospheric science and technology roadmap for 2014–2033 outlines the importance of energetic particle acceleration and transport. For example, (1) what are the origins and properties of the suprathermal seed populations of solar energetic particles? and (2) how are particles injected and accelerated throughout the heliosphere and heliosheath?

8. Conclusions

In summary, we have reviewed the Puck EPD and its design principals, heritage, advancements, and prospects on future missions. Radiation environments, where Pucks might be logical parts of the payload, require detectors and other components to be shielded, thereby increasing the launch mass associated with scientific instrumentation. Pucks have responded by becoming less resource intensive (e.g., lighter), and this paper illustrates the history and continuing advances being made in this direction. Emerging technologies and novel electrooptical designs are constantly being researched and their applicability to space instrumentation tested. We believe that the following areas of technology development are of great importance for energetic charged particle sensors in general: (1) novel TOF methods; (2) increased dynamic energy range in detectors; (3) thin foil design and implementation; and (4) ionic charge state separation for greater than several 100 s of keV/nucleon heavy ions.

Appendix A: Puck EPD Specifications

A1. Additional Instrument Details Between the Various Pucks

Quantitative specifications between the different Puck EPDs are provided in Tables A17–A3. The tables are organized such that Table A1 covers the TOF chamber and MCP details, Table A2 lists the ion and electron SSD characteristics, and Table A3 outlines the grid and foil attributes.

Table A1. TOF Chamber and MCP Detector Details

Instrument	TOF Chamber Diameter (cm)	MCP Sensitivity Area (mm^2)	MCP Pore Size (μm)	MCP Bias Angle (deg)
EPS	6	40	10	8
PEPSSI	6	40	10	8
JEDI	6	40	10	12
RBSPICE	6	40	12	12
EIS	6	40	10	12

Table A2. Ion and Electron SSD Characteristics

Instrument	SSD Thickness (μm)	SSD Deadlayer (nm)	Large Pixel Area (mm^2)	Small Pixel Area (mm^2)	Electron Flashing
EPS	1000	55	40	2	1 μm of Al
PEPSSI	500	55	40	2	1 μm of Al
JEDI	500	50	40	2	2 μm of Al
RBSPICE	500	50	40	2	2 μm of Al
EIS	500	50	40	2	2 μm of Al

Table A3. Foil and Grid Characteristics

Instrument	Collimator Foil Thickness and Composition	Start Foil Thickness and Composition (Multilayer)	Stop Foil Thickness and Composition (Multilayer)	Start and Stop Foil Grids	Collimator Grids
EPS	N/A	50 Å aluminum, 350 Å polyimide, 50 Å aluminum	100 Å palladium, 500 Å polyimide, 100 Å polyimide	40 line-per-inch with > 80% transmission	N/A
PEPSSI[a]	N/A	48 ± 25 Å aluminum, 370 ± 100 Å polyimide, 43 ± 25 Å aluminum	54 ± 25 Å palladium, 477 ± 100 Å polyimide, 45 ± 25 Å palladium	40 line-per-inch with 88% transmission	N/A
JEDI	350 Å of aluminum	50 Å carbon, 350 Å polyimide, 50 Å carbon	Same as start foil, but with additional 200 Å of aluminum	70 line-per-inch with 90% transmission	70 line-per-inch with 90% transmission
RBSPICE	620 Å of aluminum, 170 Å palladium	50 Å carbon, 350 Å polyimide, 50 Å carbon	Same as start foil, but with additional 200 Å of aluminum	>80% transmission	>80% transmission
EIS	350 Å of aluminum	50 Å carbon, 350 Å polyimide, 50 Å carbon	Same as start foil, but with additional 200 Å of aluminum	70 line-per-inch with 90% transmission	70 line-per-inch with 90% transmission

[a]Details within the certification sheet for the PEPSSI foils report the tolerances associated on the start and stop foils. These tolerances apply to the foils used in the other Puck EPDs as well.

Acknowledgments

We would like to recognize and thank the many engineers and scientists (too many to mention by name) that have contributed to the development and delivery of the Puck instruments. It is their hard work, innovative ASIC, mechanical and electrical designs, and their very long hours spent testing, calibrating, and qualifying the hardware, that have directly made the Pucks the innovative and successful instruments that they are. We would also like to acknowledge the support of APL and NASA. Data supporting this work will be made available upon request (george.clark@jhuapl.edu).

References

Allegrini, F., M. I. Desai, R. Livi, S. Livi, D. J. McComas, and B. Randol (2009), The entrance system laboratory prototype for an advanced mass and ionic charge composition experiment, *Rev. Sci. Inst.*, *80*, doi:10.1063/1.3247906.

Allegrini, F., Ebert, R. W., Fuselier, S. A., Nicolaou, G., Bedworth, P., Sinton, S., and Trattner, K. J. (2014), Charge state of ~ 1 to 50 keV ions after passing through graphene and ultrathin carbon foils, *Optical Eng.*, *53*(2), 024101, doi:10.1117/1.OE.53.2.024101.

Allegrini, F., P. Bedworth, R. W. Ebert, S. A. Fuselier, G. Nicolaou, and S. Sinton (2015), Energy loss and straggling of 1–50 keV H, He, C, N, and O ions passing through few layer graphene, *Nuclear Inst. Methods Phys. Res. B*, *358*(C), 223–228, doi:10.1016/j.nimb.2015.06.028.

Allegrini, F., R. W. Ebert, and H. O. Funsten (2016), Carbon foils for space plasma instrumentation, *J. Geophys. Res. Space Physics*, *121*, 3931–3950, doi:10.0002/2016JA022570.

Anderson, B. J., et al. (2016), Electrodynamic context of magnetopause dynamics observed by magnetospheric multiscale, *Geophys. Res. Lett.*, *43*, 5988–5996, doi:10.1002/2016GL069577.

Andrews, G. B., et al. (2007), The Energetic Particle and Plasma Spectrometer Instrument on the MESSENGER Spacecraft, *Space Sci. Rev.*, *131*(1–4), 523–556, doi:10.1007/s11214-007-9272-5.

Bagenal, F., and P. A. Delamere (2011), Flow of mass and energy in the magnetospheres of Jupiter and Saturn, *J. Geophys. Res.*, *116*, A05209, doi:10.1029/2010JA016294.

Clark, G., B. H. Mauk, C. Paranicas, P. Kollmann, and H. T. Smith (2016), Charge states of energetic oxygen and sulfur ions in Jupiter's magnetosphere, *J. Geophys. Res. Space Physics*, *121*, 2264–2273, doi:10.1002/2015JA022257.

Cohen, I. J., et al. (2016), Observations of energetic particle escape at the magnetopause: Early results from the MMS energetic ion spectrometer (EIS), *Geophys. Res. Lett.*, *43*, 5960–5968, doi:10.1002/2016GL068689.

Cravens, T. E., E. Howell, J. H. Waite Jr., and G. R. Gladstone (1995), Auroral oxygen precipitation at Jupiter, *J. Geophys. Res.*, *100*, 17,153–17,161, doi:10.1029/95JA00970.

Desai, M. I., Ogasawara, K., Ebert, R. W., McComas, D. J., Allegrini, F., Weidner, S. E., Alexander N., Livi S. A. (2015), An integrated time-of-flight versus residual energy subsystem for a compact dual ion composition experiment for space plasmas, *Rev. Sci. Inst.*, *86*(5), 054501, doi:10.1063/1.4921706.

Duvet, L., J. J. Berthelier, J. Illiano, and M. Godefroy (2000), A low-energy spectrometer with a 2π field of view for planetary missions, *Meas. Sci. Technol.*, *11*, 375–381, doi:10.1088/0957-0233/11/4/306.

Ebert, R. W., Allegrini, F., Fuselier, S. A., Nicolaou, G., Bedworth, P., Sinton, S., and Trattner, K. J. (2014), Angular scattering of 1–50 keV ions through graphene and thin carbon foils: Potential applications for space plasma instrumentation, *Rev. Sci. Inst.*, *85*(3), 033302. doi:10.1063/1.4866850.

Garrard, T. L., N. Gehrels, and E. C. Stone (1992), The Galileo Heavy element monitor, *Space Sci. Rev.*, *60*(1–4), 305–315, doi:10.1007/BF00216859.

Gkioulidou, M., A. Y. Ukhorskiy, D. G. Mitchell, T. Sotirelis, B. H. Mauk, and L. J. Lanzerotti (2014), The role of small-scale ion injections in the buildup of Earth's ring current pressure: Van Allen Probes observations of the 17 March 2013 storm, *J. Geophys. Res. Space Physics*, *119*, 7327–7342, doi:10.1002/2014JA020096.

Gloeckler, G., and J. Geiss (2004), Composition of the local interstellar medium as diagnosed with pickup ions, *Adv. Space Res.*, *34*, 53–60, doi:10.1016/j.asr.2003.02.054.

Gold, R. E., S. M. Krimigis, S. E. Hawkins III, D. K. Haggerty, D. A. Lohr, E. Fiore, T. P. Armstrong, G. Holland, and L. J. Lanzerotti (1998), Electron, proton, and alpha monitor on the advanced composition explorer spacecraft, *Space Sci. Rev.*, *86*(1–4), 541–562.

Ho, G. C., R. D. Starr, R. E. Gold, S. M. Krimigis, J. A. Slavin, D. N. Baker, B. J. Anderson, R. L. McNutt Jr., L. R. Nittler, and S. C. Solomon (2011), Observations of suprathermal electrons in Mercury's magnetosphere during the three MESSENGER flybys, *Planet. Space Sci.*, *59*(15), 2016–2025, doi:10.1016/j.pss.2011.01.011.

Ho, G. C., S. M. Krimigis, R. E. Gold, D. N. Baker, B. J. Anderson, H. Korth, J. A. Slavin, R. L. McNutt Jr., R. M. Winslow, and S. C. Solomon (2012), Spatial distribution and spectral characteristics of energetic electrons in Mercury's magnetosphere, *J. Geophys. Res.*, *117*, A00M04, doi:10.1029/2012JA017983.

Howett, C. J. A., J. R. Spencer, P. Schenk, R. E. Johnson, C. Paranicas, T. A. Hurford, A. Verbiscer, and M. Segura (2011), A high-amplitude thermal inertia anomaly of probable magnetospheric origin on Saturn's moon Mimas, *Icarus*, *216*, 221–226.

Hoyle, F. (1949), *Some Recent Researches in Solar Physics*, Cambridge Univ. Press, Cambridge, U. K.

Hughes, A. L., and V. Rojansky (1929), On the analysis of electronic velocities by electrostatic means, *Phys. Rev. Lett.*, *34*, 284–290, doi:10.1103/PhysRev.34.284.

Johnson, R. E. (1990), Energetic charged-particle interactions with atmospheres and surfaces, *Phys. Chem. Space*, 19, doi:10.1007/978-3-642-48375-2.

Johnstone, A. D. (1972), The geometric factor of a cylindrical plate electrostatic analyzer, *Rev. Sci. Inst.*, *43*, 1030–1040, doi:10.1063/1.1685826.

Jokipii, J. R. (2001), Acceleration and transport of energetic charged particles in space, *Astrophys. Space Sci.*, *277*(1/2), 15–26, doi:10.1023/A:1012212417410.

Kane, M., R. B. Decker, B. H. Mauk, and S. M. Krimigis (1998), The solar wind velocity determined from Voyager 1 and 2: Low-Energy Charged Particle measurements in the outer heliosphere, *J. Geophys. Res.*, *103*, 267–276, doi:10.1029/97JA02776.

Kasahara, S., K. Asamura, Y. Saito, T. Takashima, M. Hirahara, and T. Mukai (2006), Cusp type electrostatic analyzer for measurements of medium energy charged particles, *Rev. Sci. Inst.*, *77*, doi:10.1063/1.2405358.

Krimigis, S. M., T. P. Armstrong, W. I. Axford, C. O. Bostrom, C. Y. Fan, G. Gloeckler, and L. J. Lanzerotti (1977), The Low Energy Charged Particle (LECP) experiment on the Voyager spacecraft, *Space Sci. Rev.*, *21*(3), 329–354, doi:10.1007/BF00211545.

Krimigis, S. M., et al. (2004), Magnetosphere imaging instrument (MIMI) on the Cassini mission to Saturn/Titan, in *The Cassini-Huygens Mission*, pp. 233–329, Springer, Netherlands.

Krupp, N., et al. (2002), Leakage of energetic particles from Jupiter's dusk magnetosphere: Dual spacecraft observations, *Geophys. Res. Lett.*, *29*(15), 1736, doi:10.1029/2001GL014290.

Kunow, H., G. Wibberenz, G. Green, R. Müller-Mellin, M.-B. Kallenrode (1991), *Physics of the Inner Heliosphere II (Vol. 21)*, edited by R. Schwenn and E. Marsch, Springer, Berlin, doi:10.1007/978-3-642-75364-0.

Lagg, A., Krupp, N., Woch, J., and Williams, D. J. (2003), In-situ observations of a neutral gas torus at Europa. *Geophys. Res. Lett.*, *30*(11), 1556, doi:10.1029/2003GL017214.

Lee, C., X. Wei, J. W. Kysar, and J. Hone (2008), Measurement of the elastic properties and intrinsic strength of monolayer graphene, *Science*, *321*, 385–388, doi:10.1126/science.1157996.

Mauk, B. H. and F. Bagenal (2012), Comparative auroral physics: Earth and other planets, in *Auroral Phenomenology and Magnetospheric Processes: Earth and Other Planets*, edited by A. Keiling et al., pp. 3–26, AGU, Washington, D. C., doi:10.1029/2011GM001192.

Mauk, B. H., and S. M. Krimigis (1987), Radial force balance within Jupiter's dayside magnetosphere, *J. Geophys. Res.*, *92*, 9931–9941, doi:10.1029/JA092iA09p09931.

Mauk, B. H., S. A. Gary, M. Kane, E. P. Keath, S. M. Krimigis, and T. P. Armstrong (1996), Hot plasma parameters of Jupiter's inner magnetosphere, *J. Geophys. Res.*, *101*, 7685–7695, doi:10.1029/96JA00006.

Mauk, B. H.,et al. (2005), Energetic particle injections in Saturn's magnetosphere, *Geophys. Res. Lett.*, *32*, L14S05, doi:10.1029/2005GL022485.

Mauk, B. H., et al. (2013), The Jupiter Energetic Particle Detector Instrument (JEDI) Investigation for the Juno Mission, *Space Sci. Rev.*, 1–58, doi:10.1007/s11214-013-0025-3.

Mauk, B. H., et al. (2014), The Energetic Particle Detector (EPD) Investigation and the Energetic Ion Spectrometer (EIS) for the Magnetospheric Multiscale (MMS) Mission, *Space Sci. Rev.*, *199*, 471–514, doi:10.1007/s11214-014-0055-5.

McComas, D. J., F. Allegrini, C. J. Pollock, H. O. Funsten, S. Ritzau, and G. Gloeckler (2004), Ultrathin (~10 nm) carbon foils in space instrumentation, *Rev. Sci. Inst.*, *75*(11), 4863–4869, doi:10.1063/1.1809265.

McComas, D. J., et al. (2013), The Jovian Auroral Distribution Experiment (JADE) on the Juno Mission to Jupiter, *Space Sci. Rev.*, doi:10.1007/s11214-013-000-9.

McEntire, R. W., E. P. Keath, D. E. Fort, A. T. Y. Lui, and S. M. Krimigis (1985), The Medium-Energy Particle Analyzer (MEPA) on the AMPTE CCE Spacecraft, *IEEE Trans. Geosci. Remote Sens.*, *GE-23*(3), 230–233, doi:10.1109/TGRS.1985.289518.

McNutt, R. L. (1983), Force balance in the magnetospheres of Jupiter and Saturn, *Adv. Space Res.*, *3*(3), 55–58, doi:10.1016/0273-1177(83)90256-9.

McNutt, R. L., Jr., et al. (2008), The Pluto Energetic Particle Spectrometer Science Investigation (PEPSSI) on the New Horizons Mission, *Space Sci. Rev.*, *140*(1–4), 315–385, doi:10.1007/s11214-008-9436-y.

Mitchell, D. G., Brandt, P. C. S., Roelof, E. C., Hamilton, D. C., Retterer, K. C., and Mende, S. (2003), Global imaging of O+ from IMAGE/HENA, *Space Sci. Rev.*, *109*(1–4), 63–75, doi:10.1023/B:SPAC.0000007513.55076.00.

Mitchell, D. G., W. S. Kurth, G. B. Hospodarsky, N. Krupp, J. Saur, B. H. Mauk, J. F. Carbary, S. M. Krimigis, M. K. Dougherty, and D. C. Hamilton (2009), Ion conics and electron beams associated with auroral processes on Saturn, *J. Geophys. Res.*, *114*, A02212, doi:10.1029/2008JA013621.

Mitchell, D. G., et al. (2013), Radiation Belt Storm Probes Ion Composition Experiment (RBSPICE), *Space Sci. Rev.*, *179*(1–4), 263–308, doi:10.1007/s11214-013-9965-x.
Nichols, J. D., N. Achilleos, and S. W. H. Cowley (2016), A model of force balance in Jupiter's magnetodisc including hot plasma pressure anisotropy, *J. Geophys. Res. Space Physics*, *120*, 10,185–10,206, doi:10.1002/2015JA021807.
Oksavik, K., T. A. Fritz, Q.-G. Zong, F. Søraas, and B. Wilken (2002), Three-dimensional energetic ion sounding of the magnetopause using Cluster/RAPID, *Geophys. Res. Lett.*, *29*(9), 1347, doi:10.1029/2001GL014265.
Paranicas, C., B. H. Mauk, and S. M. Krimigis (1991), Pressure anisotropy and radial stress balance in the Jovian neutral sheet, *J. Geophys. Res.*, *96*, 21,135–21,140, doi:10.1029/91JA01647.
Paranicas, C., D. G. Mitchell, E. C. Roelof, P. C. Brandt, D. J. Williams, S. M. Krimigis, and B. H. Mauk (2005), Periodic intensity variations in global ENA images of Saturn, *Geophys. Res. Lett.*, *32*, L21101, doi:10.1029/2005GL023656.
Paranicas, C., D. G. Mitchell, S. M. Krimigis, D. C. Hamilton, E. Roussos, N. Krupp, G. H. Jones, R. E. Johnson, J. F. Cooper, and T. P. Armstrong (2008), Sources and losses of energetic protons in Saturn's magnetosphere, *Icarus*, *197*(2), 519–525, doi:10.1016/j.icarus.2008.05.011.
Paranicas, C., et al. (2014), The lens feature on the inner saturnian satellites, *Icarus*, *234*, 155–161, doi:10.1016/j.icarus.2014.02.026.
Paschalidis, N. P. (2006), A family of analog and mixed signal VLSI ASICs for NASA science missions, *Acta Astronaut.*, *59*, 974–980, doi:10.1016/j.actaastro.2005.07.044.
Paschalidis, N. P., N. Stamatopoulos, K. Karadamoglou, G. Kottaras, V. Paschalidis, E. Sarris, R. McNutt, D. Mitchell, and R. McEntire (2002), A CMOS time of flight system on a chip for spacecraft instrumentation, *IEEE Trans. Nuclear Sci.*, *49*, 1156–1163.
Paschmann, G., H. Loidl, P. Obermayer, M. Ertl, R. Laborenz, N. Sckopke, W. Baumjohann, C. W. Carlson, and D. W. Curtis (1985), The plasma instrument for AMPTE IRM, *IEEE Trans. Geosci. Remote Sens.*, *GE-23*, 262–266, doi:10.1109/TGRS.1985.289525.
Richardson, I. G. (2004), Energetic particles and corotating interaction regions in the solar wind, *Space Sci. Rev.*, *111*(3–4), 267–376, doi:10.1023/B:SPAC.0000032689.52830.3e.
Saur, J., et al. (2006), Anti-planetward auroral electron beams at Saturn, *Nature*, *439*(7077), 699–702, doi:10.1038/nature04401.
Scholer, M., F. M. Ipavich, G. Gloeckler, D. Hovestadt, and B. Klecker (1981), Leakage of magnetospheric ions into the magnetosheath along reconnected field lines at the dayside magnetopause, *J. Geophys. Res.*, *86*, 1299–1304, doi:10.1029/JA086iA03p01299.
Scholer, M., P. W. Daly, G. Paschmann, and T. A. Fritz (1982), Field line topology determined by energetic particles during a possible magnetopause reconnection event, *J. Geophys. Res.*, *87*, 6073–6080, doi:10.1029/JA087iA08p06073.
Sibeck, D. G., and R. W. McEntire (1988), Multiple satellite observations of leakage of particles from the magnetosphere, *Adv. Space Res.*, *8*(9–10), 201–216, doi:10.1016/0273-1177(88)90133-0.
Sibeck, D. G., and V. Angelopoulos (2008), THEMIS science objectives and mission phases, *Space Sci. Rev.*, *141*, 35–59, doi:10.1007/s11214-008-9393-5.
Sibeck, D. G., R. W. McEntire, A. T. Y. Lui, R. E. Lopez, S. M. Krimigis, R. B. Decker, L. J. Zanetti, and T. A. Potemra (1987), Energetic magnetospheric ions at the dayside magnetopause: Leakage or merging, *J. Geophys. Res.*, *92*, 12,097–12,114, doi:10.1029/JA092iA11p12097.
Stone, E. C., R. E. Vogt, F. B. McDonald, B. J. Teegarden, J. H. Trainor, J. R. Jokipii, and W. R. Webber (1977), Cosmic ray investigation for the Voyager missions; energetic particle studies in the outer heliosphere—And beyond, *Space Sci. Rev.*, *21*(3), 355–376, doi:10.1007/BF00211546.
Ukhorskiy, A. Y., M. I. Sitnov, D. G. Mitchell, K. Takahashi, L. J. Lanzerotti, and B. H. Mauk (2014), Rotationally driven "zebra stripes" in Earth's inner radiation belt, *Nature*, *507*(7492), 338–340, doi:10.1038/nature13046.
Van Allen, J. A. (1958), Observation of high intensity radiation by satellites 1958 Alpha and Gamma, *J. Jet Propul.*, *28*(9), 588–592, doi:10.2514/8.7396.
Williams, D. J. (1979), Magnetopause characteristics inferred from three-dimensional energetic particle distributions, *J. Geophys. Res.*, *84*, 101–104, doi:10.1029/JA084iA01p00101.
Williams, D. J., and L. A. Frank (1980), Isee 1 charged particle observations indicative of open magnetospheric field lines near the subsolar region, *J. Geophys. Res.*, *85*, 2037–2042, doi:10.1029/JA085iA05p02037.
Williams, D. J., et al. (1992), The Galileo energetic particles detector, *Space Sci. Rev.*, *60*, 385, doi:10.1007/BF00216863.
Williams, D. J., R. W. McEntire, C. Schlemm, A. T. Y. Lui, G. Gloeckler, S. P. Christon, and F. Gliem (1994), Geotail energetic particles and ion composition instrument, *J. Geomag. Geoele.*, *46*(1), 39–57.
Wolfe, J. H., R. W. Silva, and M. A. Myers (1966), Observations of the solar wind during the flight of Imp 1, *J. Geophys. Res.*, *71*, 1319–1340, doi:10.1029/JZ071i005p01319.
Young, D. T. (1998), in *Measurement Techniques in Space Plasmas-Particles*, edited by R. F. Pfaff, J. E. Borovsky, and D. T. Young, pp. 1–16 , AGU, Washington, D. C.
Young, D. T., A. G. Ghielmetti, E. G. Shelley, J. A. Marshall, and J. L. Burch (1987), Experimental tests of a toroidal electrostatic analyzer, *Rev. Sci. Inst.*, *58*, doi:10.1063/1.1139260.
Young, D. T., S. J. Bame, M. F. Thomsen, R. H. Martin, J. L. Burch, J. A. Marshall, and B. Reinhard (1988), 2π-radian field-of-view toroidal electrostatic analyzer, *Rev. Sci. Inst.*, *59*, 501–508, doi:10.1063/1.1139821.
Zelenyi, L. M., J. G. Lominadze, and A. L. Taktakishvili (1990), Generation of the energetic proton and electron bursts in planetary magnetotails, *J. Geophys. Res.*, *95*, 3883–3891, doi:10.1029/JA095iA04p03883.